PNAS RESEARCH ARTICLE | BIOCHEMISTRY ENGINEERING OPEN ACCESS

Antibody homotypic interactions are encoded by germline light chain complementarity determining region 2

Brandon Leonard[a], Kannan Sankar[a], Matthew G. Romei[a], Margaret J. Tse[b], Nina Do[a], Yanli Yang[a], Wadim L. Matochko[a], Jack Bevers[a], Sundeep Bollineni[a], Kiran Mukhyala[b], Kam Hon Hoi[a], and Greg A. Lazar[a,1]

Edited by Ira Pastan, National Cancer Institute, Bethesda, MD; received January 27, 2022; accepted April 25, 2022

The utilization of avidity to drive and tune functional responses is fundamental to antibody biology and often underlies the mechanisms of action of monoclonal antibody drugs. There is increasing evidence that antibodies leverage homotypic interactions to enhance avidity, often through weak transient interfaces whereby self-association is coupled with target binding. Here, we comprehensively map the Fab–Fab interfaces of antibodies targeting DR5 and 4-1BB that utilize homotypic interaction to promote receptor activation and demonstrate that both antibodies have similar self-association determinants primarily encoded within a germline light chain complementarity determining region 2 (CDRL2). We further show that these determinants can be grafted onto antibodies of distinct target specificity to substantially enhance their activity. An expanded characterization of all unique germline CDRL2 sequences reveals additional self-association sequence determinants encoded in the human germline repertoire. Our results suggest that this phenomenon is unique to CDRL2, and is correlated with the less frequent antigen interaction and lower somatic hypermutation associated with this loop. This work reveals a previously unknown avidity mechanism in antibody native biology that can be exploited for the engineering of biotherapeutics.

antibody engineering | homotypic interactions | receptor agonism

Avidity-driven amplification of weak transient protein–protein interactions is a common theme in immunological processes. Pathogenic targets are often highly repetitive, and antibodies have evolved architectures and structural interactions for incorporating avidity into immunological mechanisms. At a macromolecular level, these include highly valent architectures such as immunoglobulins A (IgA) (1) and M (IgM) (2) isotypes, and in less common cases, variable domain swaps that promote multivalent targeting of repeat epitopes on viral capsids (3, 4). Beyond such permanent or obligate complexes, there is increasing evidence that antibodies leverage weak homotypic interactions to increase avidity, often in a manner in which self-association is coupled energetically to target binding. Examples include the transient hexamerization of the Fc region that enhances IgG effector mechanisms (5) and Fab–Fab interactions that augment neutralization against repeat glycan or protein epitopes on viral capsids (6) and plasmodium (7–9). Recent structural insights suggest Fab–Fab interactions may contribute to the therapeutic mechanism of the clinically successful anti-CD20 antibody rituximab (10). A better understanding of the transient protein–protein interactions encoded by antibody repertoires is needed to better understand their role in natural immune response, as well as enable their potential utility for biotherapeutic optimization.

Significance

Weak transient interactions are fundamental to immune responses, enabling avidity-driven triggers for pathogen neutralization and cellular regulation. In contrast to obligate binding interactions that can be directly investigated structurally, the low or transitory abundance of weak interactions make them difficult to identify and characterize. This study leverages receptor agonism systems that are sensitive to oligomerization to investigate transient homotypic interfaces between antibody Fab regions. Our results show that self-association determinants are encoded naturally by the antibody germline through light chain complementarity determining region 2 (CDRL2), and these determinants can be engineered into antibodies to enhance their therapeutic properties. Insights into avidity-driven interactions create opportunities for optimization, and accordingly this work expands the engineering toolbox for antibody-based drugs.

Results

Structure-activity relationship mapping of a homotypic antibody interaction. We investigated the structural and functional determinants of homotypic interaction in a previously reported antibody referred to as KMTR2 that targets death receptor 5 (DR5, TRAIL-R2, and TNFRSF10B), a member of the tumor necrosis factor receptor superfamily (TNFRSF). Members of this class generally require receptor clustering on the cell surface to drive signaling and, as a consequence, antibody agonists are typically dependent on extrinsic crosslinking for activity (e.g., via secondary antibody reagents or antibody Fc interactions with immune cell Fc receptors). However, the KMTR2 antibody has a unique ability to cluster and agonize receptors without the requirement for extrinsic crosslinking, enabling it to intrinsically promote potent in vitro apoptotic signaling and in vivo tumor regression (11). KMTR2 exists as a monomer in solution, and clustering is mediated through a distinctive homotypic interface that is tightly coupled with target engagement (12). We further delineated the determinants of this unique property at the sequence, structural, and functional levels.

Competing interest statement: The authors declare a competing interest. All authors are current or former employees of Genentech, a member of the Roche Group, and are shareholders in Roche. This study was supported by internal Genentech funds, and the funders had no role in study design, data collection and analysis, decision to publish, or preparation of the manuscript.

This article is a PNAS Direct Submission.

[1]To whom correspondence may be addressed. Email: lazarg@gene.com.

This article contains supporting information online at http://www.pnas.org/lookup/suppl/doi:10.1073/pnas.2201562119/-/DCSupplemental.

Published June 2, 2022.

A striking feature of KMTR2 is that its sequence is highly similar to germline, with a light chain variable region (VL) that shares 100% identity with IGKV3-11 (Fig. 1*A* and *SI Appendix*, Fig. S1*A*). Inspection of the crystal lattice from the previously solved structure of KMTR2 in complex with the DR5 extracellular domain (ECD) revealed an interface between the two copies of the KMTR2 Fabs comprised principally of its light chain (12) (Fig. 1*B*). Using a distance cutoff of 4 Å between opposing Fabs, we identified 18 residues within close proximity located predominantly in either CDRH3 or CDRL2 and its nearby framework regions (*Inset* sticks in Fig. 1*B*). We constructed a panel of 75 variants of KMTR2 with mutations at these residues (*SI Appendix*, Table S1). Variant antibodies were produced to high purity and characterized for DR5 binding assessed using surface plasmon resonance (SPR) and intrinsic cell death activity against DR5^{+} Colo205 cells. Of particular interest were variants, illustrated by N53R as described previously (12), that are not involved in antigen binding yet lose intrinsic activity, implicating them in the homotypic interface (*SI Appendix*, Fig. S2*A*).

Our structure-activity relationship (SAR) study enabled functional separation of antigen binding from the Fab–Fab interface for most of the germline encoded IGKV3-11 light chain (Fig. 2*A*). Only two mutations at D50 abrogated DR5 affinity (*Lower Right* blue box). The larger panel of mutants that retained DR5 binding fell into two groups, those that retained activity (*Upper Left* red box), and those that lost agonist activity (*Lower Left* green box). The latter residues, most of which reside in and proximal to CDRL2, are implicated in stabilization of the Fab–Fab interface. Mutation of selected residues in the heavy chain, which primarily reside in CDRH3, revealed an entanglement of binding and self-association at these positions (Fig. 2*B*). Because of this, and the virtually universal requirement of CDRH3 for target engagement, we did not explore this motif further as part of our engineering approach (below).

A similar homotypic interaction was revealed in an antibody of distinct specificity. KMTR2 is a phage-derived antibody, and conventional in vitro panning selects for target binding, not agonist activity. The distinctive nature of its Fab–Fab interface and yet complete identity to IGKV3-11 suggested an inherent propensity for homotypic interaction encoded by the germline. A light chain search of the Protein Data Bank (PDB) led us to the anti-4-1BB (CD137 and TNFRSF9) antibody urelumab, which is identical to the IGKV3-11 germline with the exception of a 2-aa insertion in CDRL3 (Fig. 1*A*). Expansion of the crystal lattice of the previously solved structure of urelumab (13) revealed inter-Fab packing of opposing symmetry mates (Fig. 1*B*). Similar to KMTR2 the Fab–Fab interface of urelumab is also mediated principally by CDRL2, yet in a slightly different configuration. In KMTR2 the CDRL2 loops of the opposing Fabs interact in an anti-parallel fashion with the central residues of CDRL2 in closest proximity (Fig. 1*B*).

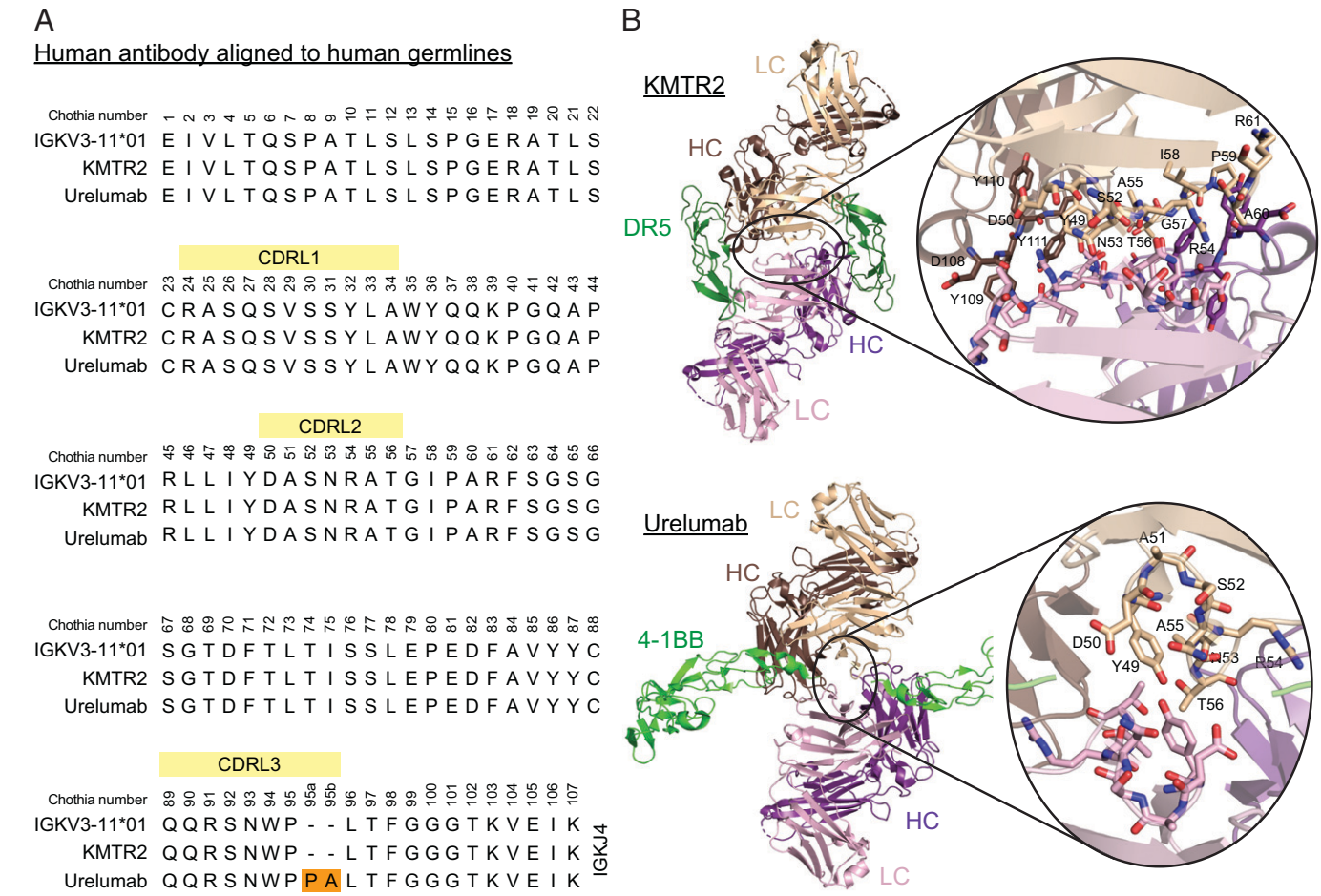

Fig. 1. Germline alignment and structural determinants for homotypic interactions of agonist anti-DR5 and anti-4-1BB antibodies. (*A*) Alignment of the KMTR2 and urelumab light chain variable regions to the nearest germline sequences. CDRs are indicated above the aligned sequence. Deviations from germline are highlighted in orange. (*B*) Crystal structures of two KMTR2 Fabs in complex with two DR5 molecules (*Top*) and two urelumab Fabs in complex with two 4-1BB molecules (*Bottom*). For KMTR2, residues shown with sticks are those within 4 Å of the opposing Fab or antigen. For urelumab, Chothia light chain residues 49–56 are shown with sticks.

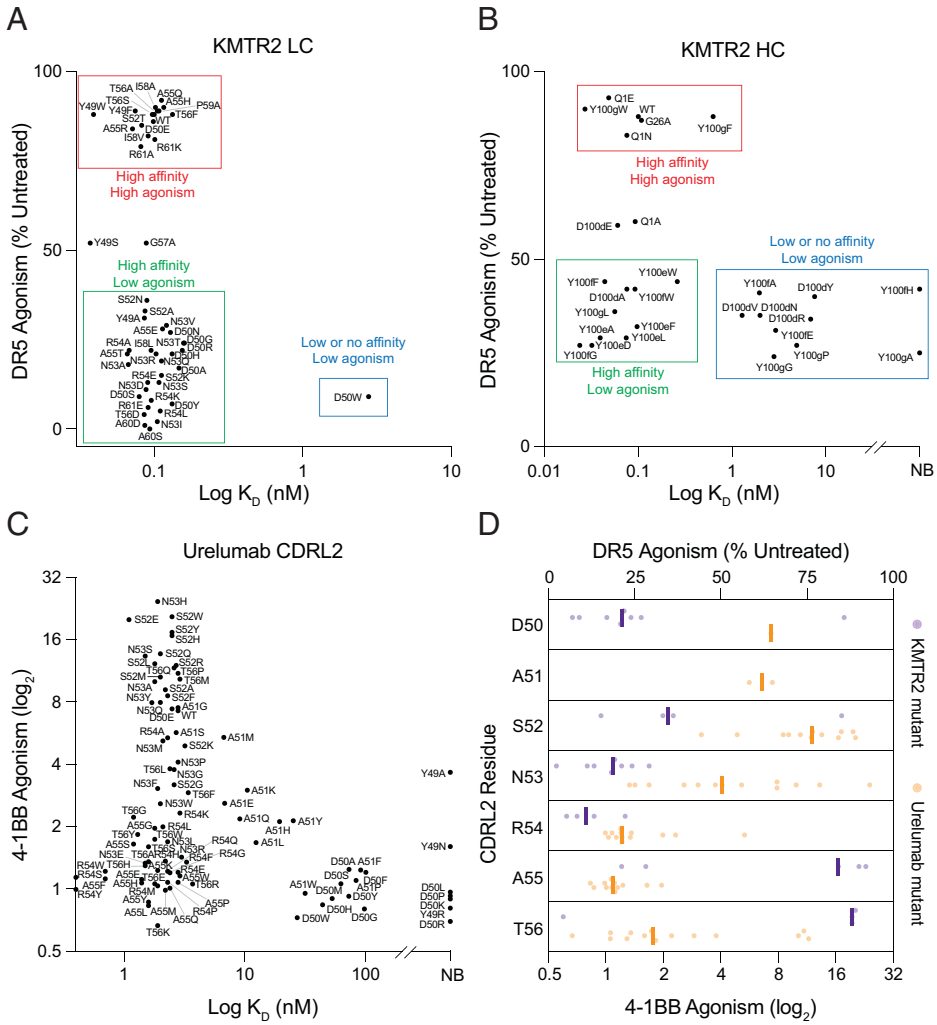

Fig. 2. SAR Analysis of anti-DR5 and anti-4-1BB antibodies. (*A* and *B*) Plot of DR5 affinity vs. agonism as assessed by the induction of cell death of COLO205 cells treated with 1 nM antibody for the indicated light chain (*A*) and heavy chain (*B*) mutants of KMTR2 reveals three general groups of variants. Mutations in the lower right quadrant (blue) reduce binding and agonist activity; while these sites may be important for mediating Fab–Fab contacts, the loss of affinity precludes conclusion. Mutations in the upper left quadrant (red) maintain both affinity and activity, indicating that they are neither important for DR5 binding nor self-association. Mutations in the lower left quadrant (green) are of greatest interest, as these sites have modest or no effect on DR5 affinity, yet show substantially reduced intrinsic agonist activity, implicating these residues as contributing to the Fab–Fab interface. NB indicates no binding or binding below the threshold needed to achieve a reliable kinetic fit. (*C*) Plot of 4-1BB affinity vs. agonism as assessed by fold change in luciferase reporter signal of 4-1BB expressing Jurkat cells treated with 0.8 nM antibody for the indicated CDRL2 variants. (*D*) Plot of cell activity for all CDRL2 variants of KMTR2 (purple, top axis, DR5 agonism) and urelumab (orange, bottom axis, 4-1BB agonism) that maintain near wildtype affinity for DR5 or 4-1BB, respectively. The purple and orange lines represent the median value at each position.

The urelumab homotypic Fab interface has fewer contacts within the middle of CDRL2, but Y49 and the C-terminal residues of CDRL2 show the closest proximity to the opposing Fab (Fig. 1*B*).

Given the structural similarities of Fab–Fab interaction and the germline nature of the light chains, together with our KMTR2 data implicating CDRL2, we performed a similar SAR study on urelumab. A series of 94 mutations were engineered at residues 49–56 of the light chain and tested for both 4-1BB binding and agonist activity in a cell-based luciferase reporter assay. N53R again exemplified the variant set with respect to contribution to the homotypic interaction, maintaining antigen affinity yet abrogating the antibody's intrinsic ability to cluster and consequently agonize receptor (*SI Appendix*, Fig. S2*B*). The results from this full SAR study were less clear-cut for some residues, with mutations at Y49 and the N-terminal end of the urelumab CDRL2 disrupting antigen binding, making their contribution to the Fab–Fab interface difficult to determine (Fig. 2*C*). Nonetheless, several mutations resulted in decreased activity without impacting affinity. Consistent with the interactions observed in the crystal lattice, the C-terminal end of the urelumab CDRL2 was an evident contributor to the Fab–Fab interface for this antibody. A plot of all CDRL2 variants that maintain antigen affinity for both antibodies underscores the central contribution of this region to Fab–Fab interaction, yet highlights their different binding modes (Fig. 2*D*). In particular, the N-terminal and central residues of the KMTR2 CDRL2 were the most sensitive to mutation while the C-terminal end of the urelumab CDRL2 was the main determinant of its Fab–Fab interface. Overall, these studies define a related homotypic interaction in two distinct antibodies mediated primarily by CDRL2 that is responsible for their unique intrinsic agonist potential against their respective target receptors.

Transfer of interaction determinants to other antibodies leads to enhanced activity. To more rigorously investigate the germline IGKV3-11 light chain interface, we explored its engineering utility. We systematically transferred the light chain self-association determinants into a panel of 11 humanized anti-OX40 (CD134, TNFRSF4) antibodies as an "acceptor set." OX40 also requires

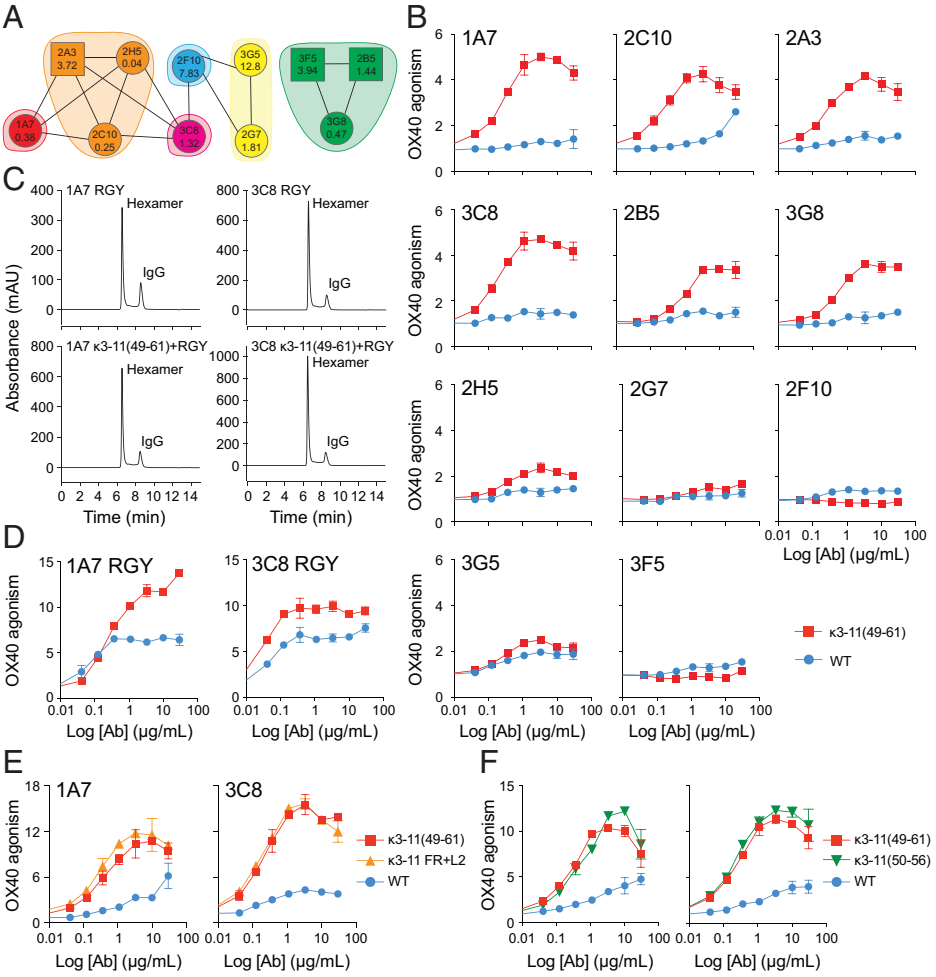

Fig. 3. IGKV3-11 CDRL2 grafted anti-OX40 antibodies are superior receptor agonists. (*A*) Epitope binning and affinities of a panel of in-house derived anti-OX40 antibodies using array-based SPR imaging (CFM/IBIS, Carterra). Each node is a different antibody clone and shaded regions show clones belonging to the same epitope bin. Black lines between nodes indicate overlapping epitopes. Square and circular nodes denote the availability of one- and two-way binning data, respectively. All affinities are K_D in nM and shown below the clone name. (*B*) OX40 agonism of wild-type (WT) or κ3–11(49-61) grafted anti-OX40 antibodies. The graphs show relative NF-κB luciferase signal in an OX40 overexpressing Jurkat reporter. (*C and D*) SEC profiles (*C*) and OX40 agonism (*D*) of RGY hexamer inducing variants of 1A7 with and without κ3-11(49–61). No crosslinker was used in the activity assay. (*E and F*) OX40 agonism for the indicated WT, κ3-11(49–61), and κ3-11 FR+L2 (*E*) or κ3-11(50-56) (*F*) grafted anti-OX40 clone.

higher-order clustering for signaling, and receptor activation by agonist antibodies is highly sensitive to oligomerization (14). Characterization of the binding properties of this antibody panel demonstrated that they bound to 6 overlapping epitopes along human OX40 (hOX40) with K_D values ranging from 0.13 to 13.8 nM (Fig. 3*A* and *SI Appendix*, Table S2). We first grafted the entire IGKV3-11 CDRL2 extended interface (referred to as κ3-11 (49–61)) onto the 11 anti-OX40 antibodies and assessed activity in a cell-based assay utilizing a Jurkat cell line engineered to express OX40 and a nuclear factor κB (NF-κB) luciferase reporter. A total of 6 out of 11 of the grafted clones showed strong OX40 receptor agonism, albeit still in the presence of extrinsic crosslinking, where activity was rarely or weakly observed for the parental antibodies (Fig. 3*B*). As an additional control, an irrelevant (anti-Her2) antibody showed no activity across a full dose range over no antibody control (*SI Appendix*, Fig. S3). No apparent correlation was observed between enhanced OX40 agonism and affinity or epitope bin for this panel of κ3-11 engrafted anti-OX40 clones (*SI Appendix*, Fig. S4). Taken together, these results suggest that the homotypic association propensity of IGKV3-11 CDRL2 is a transferable property with respect to antibody sequence and target specificity.

While homotypic association may be advantageous from an activity standpoint, its potential impact on solution properties and therapeutic developability is a concern. A preliminary molecular assessment of aggregation, stability, and surrogate viscosity suggested that κ3-11 CDRL2 engraftment introduces no apparent developability liabilities relative to the parental antibody (*SI Appendix*, Fig. S5).

Previous work revealed a homotypic interaction in the antibody Fc region that mediates transient IgG hexamer formation (5). Engineered Fc variants at this interface that promote hexamers in solution can enable receptor agonism in the absence of extrinsic crosslinking (14–16). We explored whether κ3-11 grafts could synergize with the triple Fc hexamer variant E345R/E430G/S440Y (RGY) to further enhance intrinsic agonist activity. RGY variant versions of κ3-11(49–61)-grafted 1A7 and 3C8 antibodies did not alter solution hexamer formation as compared to the parental antibodies (Fig. 3*C*), but promoted higher levels of intrinsic agonism in the Jurkat-OX40-NF-κB luciferase reporter assay (Fig. 3*D*). These data suggest that CDRL2- and Fc-mediated self-association can synergize to enhance avidity-driven agonist mechanisms.

Enhanced activity is driven principally by CDRL2 and is not a consequence of affinity variance. To determine whether additional IGKV3-11 light chain framework residues outside of κ3-11(49–61) can contribute to the formation of the Fab–Fab interface, we grafted the entire IGKV3-11 light chain framework

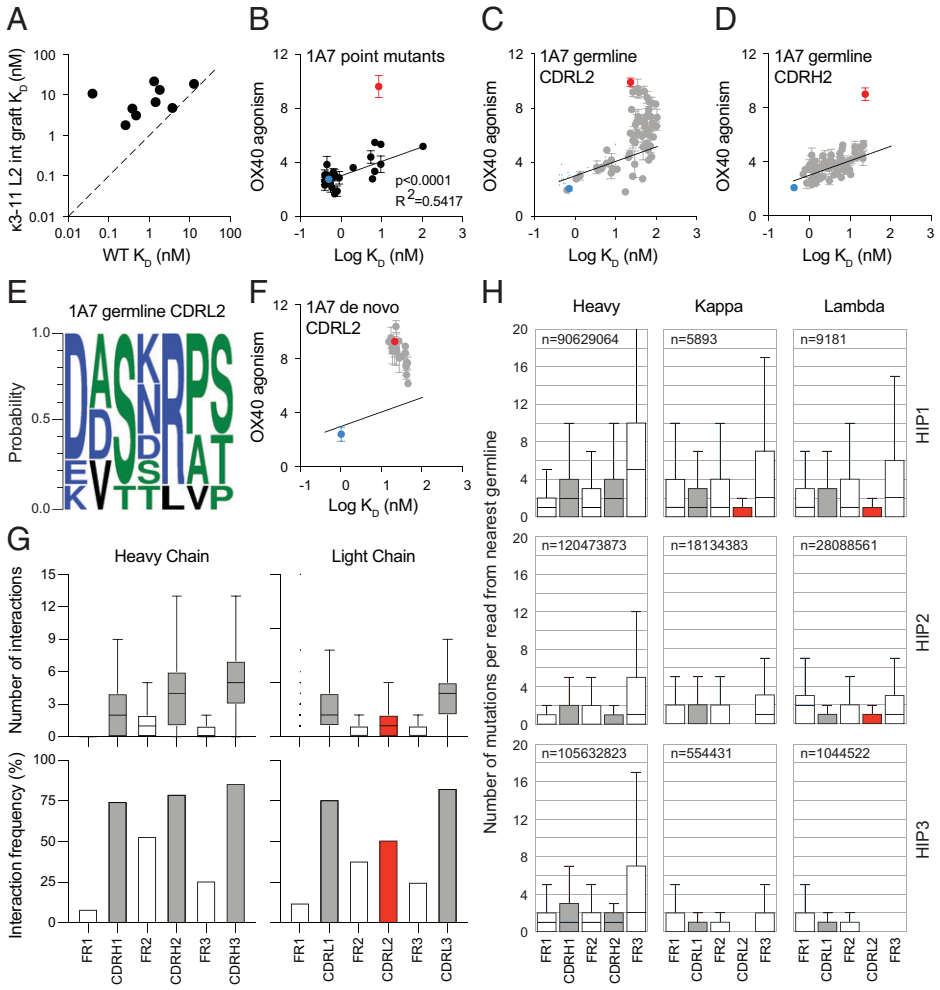

Fig. 4. Homotypic interaction is broadly encoded in germline CDRL2 sequences and associated with decreased canonical CDR functionality. (*A*) Relationship between affinity measurements for wild-type (WT) and κ3-11 L2 grafted anti-OX40 antibodies. The dashed black line indicates a 1–1 correlation between affinities of WT and κ3-11(49-61) grafted antibodies. (*B–D*) Correlation between affinity and OX40 receptor agonism for a panel of 1A7 light and heavy chain point mutants (*B*), 1A7 germline CDRL2 grafts (*C*), and 1A7 germline CDRH2 grafts (*D*). (*E*) Sequence logo of CDRL2 for the top hits from the germline CDRL2 engrafted 1A7 variants. (*F*) Correlation between affinity and OX40 receptor agonism for de novo designed CDRL2 sequence grafts. In each graph in (*B*)–(*D*), and (*F*) the solid line black represents a linear regression of the point mutant and WT data from (*B*). WT 1A7 is shown in blue, κ3-11(50–56) grafted 1A7 is shown in red, point mutants are shown in black, and all other grafted antibodies are shown in gray. (*G*) The number (*Top*) and frequency (*Bottom*) of antigen interactions between each framework (FR) and complementarity determining region (CDR) of the variable domain of the heavy (*Left*) and light (*Right*) chain for all Fab:antigen structures in the PDB. For the boxplots, the box describes the interquartile range of 25th to 75th percentile, the bar within the box denotes the median value, and the whisker is 1.5x of the interquartile range and serves as the boundary for outliers. (*H*) The mutational landscape for each region on the v-gene segment for three healthy adult human subjects, HIP1, HIP2, and HIP3. The number of mutations represents the number of nucleotide differences per read from the nearest human germline. The total number of reads analyzed (n) is indicated in the upper left corner of each graph. The elements of each box plot are the same as those in (*G*).

and CDRL2 onto the 1A7 and 3C8 antibodies (κ3-11 FR+L2). No further improvement in activity was observed upon the addition of the IGKV3-11 framework into these antibodies, again indicating that the most important determinants of this interface are residues in and proximal to CDRL2 (Fig. 3*E*). We also asked if the entire κ3-11(49–61) graft was necessary to improve the activity observed in the context of the anti-OX40 panel. Truncation of the engrafted sequence to the Chothia-defined IGKV3-11 germline CDRL2 containing residues 50–56 was sufficient to induce equivalent activity as the κ3-11(49–61) graft in the 1A7 and 3C8 antibodies (Fig. 3*F*).

Prior work has shown that the affinity of an antibody for its target can inversely correlate with receptor agonism (17). Unsurprisingly, grafting of κ3-11(49–61) resulted in varying losses of binding affinities across the panel of engineered anti-OX40 antibodies (Fig. 4*A* and *SI Appendix*, Table S2). To rigorously distinguish between the putative self-association mechanism and the affinity-dependence of OX40 agonism, we compared the agonist activity of the grafted 1A7 antibody to that of a panel of 19 1A7 heavy and light chain point mutants spanning an affinity range of over 100-fold. We observed a correlation between increased receptor agonism and decreased affinity for the panel of point mutants, albeit a modest one (Fig. 4*B* and *SI Appendix*, Table S3). Importantly, the κ3-11(50–56)-grafted antibody demonstrated significantly higher agonist activity compared to all other variants, including those with similar affinity (Fig. 4*B*). Together, these data show that the improved activity of the graft variant is not due merely to decreased affinity.

Homotypic interactions are broadly encoded within germline CDRL2 sequences. The germline nature of the IGKV3-11 CDRL2 interface suggests a natural propensity for homotypic interaction, and we were intrigued by the prospect that such interfaces may be more broadly encoded within the human germline, specifically at CDRL2. To test this hypothesis, we grafted every unique germline CDRL2 sequence in the human repertoire onto

the 1A7 antibody and assessed their activity in the OX40 agonism assay that is sensitive to receptor clustering. A plot of affinity vs. activity for each graft revealed that many germline CDRL2 grafts promoted activity that substantially exceeded the affinity-activity correlation, with the IGKV3-11 CDRL2 graft being the most optimal (Fig. 4*C* and *SI Appendix*, Table S4). As a control, we also grafted all unique germline heavy CDR2 (CDRH2) sequences onto the heavy chain of 1A7. CDRH2 was chosen as the least likely to abolish OX40 binding based on the crystal structure of 1A7 bound to the receptor ECD (14). Here, we found that activity of the CDRH2 grafts tracked strictly with affinity, mirroring the results of the point mutants and showing again that the IGKV3-11 CDRL2 graft is an outlier to the activity-affinity relationship (Fig. 4*D* and *SI Appendix*, Table S5). Taken together, these data suggest that homotypic interactions are more broadly encoded within germline CDRL2 sequences and that the mechanism is not common to all CDRs.

Examination of the top hits from the germline CDRL2 graft data revealed a sequence-dependence associated with increased agonist activity (Fig. 4*E*). Based on this analysis, we designed 21 de novo CDRL2 sequences in an attempt to further optimize the Fab–Fab interaction. The set of de novo CDRL2 sequences was indeed biased toward enhanced self-association beyond that expected from the activity–affinity relationship, with the IGKV3-11 CDRL2 graft remaining one of the most active among this panel (Fig. 4*F* and *SI Appendix*, Table S6).

CDRL2-mediated homotypic interaction is correlated its lower contribution to antigen binding. If Fab homotypic interaction is a germline-encoded function of CDRL2, we surmised that CDRL2 would be less involved in antigen interactions to permit self-association in this region, and further that CDRL2 somatic hypermutation would be low in order to maintain Fab–Fab interaction during B cell clonal selection, which could offer a selective advantage for B cell receptor (BCR) clustering and downstream signaling. To test these hypotheses, we took two independent informatic approaches. First, we assessed intermolecular interactions at each CDR residue across all Fab-antigen cocrystal structures in the PDB. Consistent with previous reports (18, 19), we observed that CDRL2 is the least involved CDR in antigen binding both in terms of number and frequency of interactions (Fig. 4*G*). Second, we performed a CDR-specific mutational analysis utilizing a previously published dataset of antibody repertoire sequences from three individual patients. The results show that CDRL2 naturally has the fewest mutations from the nearest germline sequence relative to all other CDR and framework regions (Fig. 4*H*).

Discussion

While obligate binding interactions, such as those between antibody and antigen, are readily investigated with direct structural methods such as crystallography and cryo-electron microscopy, many interactions that contribute to immunological recognition are weak or transient, making them harder to identify due to low or transitory abundance. Yet, weak interactions are as fundamental to immune response as obligate ones, enabling conversion of an avid cell synapse or antibody complex into a cooperative biochemical trigger for cellular activation or inhibition. In this work, we have leveraged receptor agonism systems that are sensitive to oligomerization to investigate transient homotypic interfaces between antibody Fab regions. The common germline yet different binding modes of the KMTR2 and urelumab Fab–Fab interactions, together with the affinity and epitope diversity of the anti-OX40 acceptor set are consistent with a mechanism that has evolved to permit homotypic interaction across diverse naturally selected antibodies. The ability of multiple germline CDRL2 sequences to mediate effects may reflect a natural design to cosample avidity and epitope diversity. Germline-encoded homotypic interaction through CDRL2 would enable avidity contributions at the BCR and antibody stages of humoral immunity. Beyond their role in biology, native interfaces are common starting points for protein engineering, and indeed many clinically successful antibody platforms are optimizations of natural biological interactions. In this frame, the present work not only reveals a previously uncharacterized antibody avidity mechanism but also advances an additional naturally encoded interface that can potentially be exploited to enhance the activities of biotherapeutic medicines.

Materials and Methods

KMTR2 and urelumab SAR studies. Symmetry mates of the KMTR2 Fab/DR5 complex (PDB: 3X3F) (12) and urelumab/4–1BB complex (PDB: 6MHR) (13) were generated using PyMOL and the Fab–Fab dimer structure was extracted. For KMTR2 variant design, all contacts between the two copies of Fabs were identified using a distance cutoff of 4 Å between heavy atoms. Mutations were design based on similarity and dissimilarity to the native residue, as well as in some cases the amino acid identity at the same position in the OX40 antibody panel (*SI Appendix*, Table S1). Urelumab variants were designed at residues 49–56. Mutations were generally made to alanine and dissimilar residues from the native that explored chemical diversity with a limited number of mutations.

Genes encoding the variable heavy and light regions were constructed using gene synthesis (Genewiz/GenScript) and cloned in the pRK mammalian expression vector (20) with human Ckappa and human IgG1 constant chains. Variants were constructed using PCR-based mutagenesis. Antibody heavy and light chain DNAs in pRK vector were cotransfected into CHO or 293 cells for expression of KMTR2 and Urelumab, respectively. Antibodies were purified using MabSelect SuRe column (GE Healthcare, #17-5438-01). Protein quality was assessed by size exclusion chromatography using a Waters xBridge BEH200A SEC 3.5 μm (7.8 × 300 mm) column (Waters, 176003596). Antibodies were purified to monomeric species with negligible higher order species, and remained monodisperse in solution after purification.

DR5 agonism assay. For anti-DR5 assays, human COLO205 cells were plated at 100,000 cells/well of a 96-well white walled plate (Corning) in 50 μL of RPMI supplemented with 1% L-glutamine and 10% heat inactivated fetal bovine serum (HI FBS) and allowed to adhere overnight under 5% CO_2 at 37 °C. Dilutions of antibodies were prepared in growth media at 2 nM and 50 μl of each antibody sample was added to each well (1 nM final concentration). To assess cell viability, cells were incubated with antibody for 24 h prior to the addition of CellTiter-Glo (Promega). Experiments were done in triplicate, and luminescence was read using a Perkin-Elmer Envision plate reader.

4-1BB agonism assay. Engineered Jurkat T cells that express human 4-1BB and a luciferase reporter were obtained from Promega (cat. #JA2351). Urelumab mutants were serially diluted in 20 μL RPMI containing 1% L-glutamine and 10% HI FBS at 2x concentration in 384-well tissue culture plates (Corning Inc., cat. #3764). A total of 40,000 4-1BB luciferase reporter cells were added to each well in 20 μL. The plates were then incubated for 16–18 h under 5% CO_2 at 37 °C. Forty microliters of Bright Glo (Promega, cat. #E2610) was then added to each well and incubated with shaking at room temperature for 5 min. Luminescence was detected using a Perkin-Elmer Envision plate reader. This process was automated using a Tecan Fluent. Activity data from this assay are reported as fold change over a no-antibody control.

Affinity measurements and epitope mapping. An array-based SPR imaging system (CFM/IBIS) was used to analyze binding kinetics of the KMTR2 SAR mutants and epitope bin the anti-OX40 antibody panel. Purified antibodies were diluted at 10 μg/mL in 10 mM sodium acetate buffer pH 4.5, and amine coupling with a Continuous Flow Microspotter (CFM) was used to directly immobilize the antibodies onto an SPR sensorprism CMD 200M chip (XanTec

Bioanalytics). For both kinetics and binning experiments, the IBIS MX96 SPRi (Carterra) was used to evaluate binding to the arrayed antibodies. All experiments were performed at 25 °C in a 10 mM Hepes, pH 7.4, 150 mM NaCl, 3 mM EDTA, and 0.005% vol/vol Surfactant P20 running buffer (HBS-P, GE). For kinetics analysis of the KMTR2 SAR mutants, each point of a 3-fold concentration series of DR5 starting at 300 nM was injected for 3 min and allowed to disassociate for 10 min. The surface was regenerated between cycles with 10 mM glycine pH 1.7, and the data were processed using Scrubber (BioLogic Software). D100dR (HC), Y100eD (HC), Y100gW (HC), and D50R (LC) had detectable binding with kinetics similar to other related mutants, but with low response units. Therefore, the model fits for these mutants had inherently more error than the others. For binning of the anti-OX40 antibody panel, human OX40 (G&P Bioscience, FCL-2479) was first injected for 4 min at 100 nM followed by a second 4-min injection of purified antibody at 10 μg/mL in HBS-P running buffer. The surface was regenerated between cycles with 10 mM Glycine pH 1.7. Binning data were processed using the Epitope Binning software tool (Carterra).

Solution affinity constants for the urelumab variant panel and engrafted anti-OX40 antibodies were assessed using either a Biacore T200 or Biacore 8K+ instrument (GE). In both cases, antibodies were captured using a Series S Protein A chip (GE) according to the manufacturer's specifications. A serial dilution of 4-1BB or OX40 (G&P Bioscience, FCL-2479) was prepared in HBS-P and injected for 3 min, followed by 5-min dissociation. Affinity constants were obtained through kinetic fitting using the Biacore Evaluation Software (GE).

Engineering of anti-OX40 antibodies. Variable regions for the anti-OX40 panel were derived in-house. All anti-OX40 light chain sequences were aligned to the IGKV3-11 germline light chain from KMTR2. For IGKV3-11 CDRL2 extended interface (κ3-11(49–61)) and IGKV3-11 CDRL2 (κ3-11(50–56)) grafts, the indicated Chothia defined residues from the IGKV3-11 germline sequence were used to replace the corresponding residues in the indicated anti-OX40 antibody light chains. For grafts containing CDRL2 and the entire framework from IGKV3-11 (FR+L2), CDRL1 and CDRL3 from 1A7 and 3C8 were grafted into the IGKV3-11 germline sequence. For the analysis of all germline CDRL2 sequences, CDRL2 in the anti-OX40 clone 1A7 was replaced with each unique CDRL2 sequence present in the human germline. Likewise, CDRH2 in 1A7 was replaced with each unique germline CDRH2 sequence. Molecular biology was carried out using gene synthesis (Genewiz/GenScript).

To make hexameric variants of 1A7 and 3C8, E345R/E430G/S440Y (RGY) mutations were introduced into the Fc region of the heavy chain using QuikChange Lightning Multi Site-Directed Mutagenesis Kit (Agilent, cat. 210514).

For anti-OX40 expression and purification, pRK vectors encoding antibody heavy and light chain DNAs encoding anti-OX40 antibodies in pRK vector were cotransfected into Expi293 cells for expression. Antibodies were purified using MabSelect SuRe column followed by SEC using a HiLoad 16/600 Superdex 200 column as described previously (14). Protein quality was assessed by size exclusion chromatography using a Waters xBridge BEH200A SEC 3.5um (7.8 × 300 mm) column (Waters, 176003596). Molecular weight of all antibodies and proteins was confirmed by liquid chromatography–mass spectrometry. All antibodies tested were purified to monomeric species with negligible higher order species, and remained monodisperse in solution after purification.

Affinity data, activity data, and, where appropriate, graft sequences are provided for all engineered variants in *SI Appendix*, Tables S2–S6.

OX40 agonism assay. OX40 overexpressing Jurkat cells engineered with an NF-κB luciferase reporter as previously reported (14). Antibody formats and goat anti-human IgG Fcγ fragment-specific crosslinking antibody (Jackson ImmunoResearch Laboratories Inc., cat. #109-005-098) were serially diluted together at a 1:1 molar ratio and at 2x concentration in RPMI containing 1% L-glutamine and 10% HI FBS. Twenty microliters of the antibody solution was combined with 20 μl of reporter cells resuspended in media to give a final concentration of 80,000 cells/well in 384 well plates (Corning, cat. #3764). The plates were then incubated for 16–18 h under 5% CO_2 at 37 °C. A total of 40 μl of Bright Glo (Promega, cat. #E2610) was then added to each well and incubated with shaking at room temperature for 10 min. Luminescence was detected using a Perkin-Elmer Envision plate reader. For larger panels of antibodies, automation of this assay was developed using a Tecan Fluent. All assays were performed in the presence of a 1:1 molar ratio of crosslinking antibody unless otherwise indicated and activity data from this assay is reported as fold change over a no-antibody control.

Sequence logo parameters and de novo CDRL2 sequence design. The sequence logo of the CDRL2 grafts was scaled between zero and one based on the activity readouts of the various germline CDRL2 grafts in the Jurkat-OX40-NF-κB luciferase assay. Consequently, the logo demonstrated both the diversity of the germline CDRL2 grafts tested as well as the propensity for each positional amino acid to contribute to activity. The bigger the amino acid letter on the logo plot, the stronger its contribution toward the activity readouts. For logo generation, the activity readouts were z-score standardized and then translated to contain all positive values and the minimum at 1. Each positional amino acids' value was aggregated and the proportion was determined per amino acid per position. This proportion value was referenced to generate the sequence logo. The de novo CDRL2 sequence design was determined based on the per position maximum valued amino acid to result in the final 7-mer CDRL2 design.

Structural analysis of Fab-antigen interactions. Fab-antigen protein structures were first identified by running igblastp v1.17 (21) on atomic sequences extracted from PDB files (22) with an E-value cutoff of 1e–10. The sequences from Fab structures were then annotated with the AHo numbering scheme (23) for the variable domain using ANARCI vFeb 2010 (24). This numbering scheme was then mapped to the Fab-antigen interface residues for all interfaces identified by the PISA program from the CCP4 suite v1.7 (25). We used the VH-antigen and VL-antigen interface with the largest interaction surface identified by PISA to select the VH-antigen and VL-antigen interface for each structure. Mapping the antigen interacting residues identified by PISA to a reference numbering system enabled comparison of the interaction frequencies of reference positions on the variable domain across all Fab structures.

Sequence analysis of CDRL2 diversity. In order to assess the somatic mutation landscape for each of the regions on the v-gene segment of the human adult antibody repertoire, three healthy adults' NGS variable heavy, kappa, and lambda chain sequences were obtained from the Human Immunome Program (26). Antibody variable domain sequences were aligned to the human antibody germline database using IgBLAST (21). Variable domain sequences were assigned with the top hit germline. In order to determine somatic mutations, assigned germlines were used as templates for pairwise alignment with query sequences. The number of nucleotide differences was determined to be the number of somatic mutations. The distribution of the mutational landscape for each chain in each adult was plotted as box-plots.

Data Availability. All study data are included in the article and/or *SI Appendix*.

ACKNOWLEDGMENTS. The authors thank, Grace Wang, Randall J. Brezski, Kellen Schneider, Jia Wu, Dhaya Seshasayee, Yongmei Chen, Nancy Chiang, Gerald Nakamura, May Lin, Peter Luan, Farzam Farahi, Ingrid Kim, and Avinash Gill for technical contributions.

Author affiliations: [a]Department of Antibody Engineering, Genentech Inc., South San Francisco, CA 94080; and [b]Department of Structural Biology, Genentech Inc., South San Francisco, CA 94080

Author contributions: B.L., K.S., M.G.R., M.J.T., W.L.M., K.M., K.H.H., and G.A.L. designed research; B.L., K.S., M.G.R., M.J.T., Y.Y., W.L.M., J.B., and K.H.H. performed research; N.D. and S.B. contributed new reagents/analytic tools; B.L., K.S., M.G.R., M.J.T., Y.Y., J.B., K.H.H., and G.A.L. analyzed data; and B.L., K.S., M.G.R., K.M., K.H.H., and G.A.L. wrote the paper.

1. Z. Wang *et al.*, Enhanced SARS-CoV-2 neutralization by dimeric IgA. *Sci. Transl. Med.* **13**, eabf1555 (2021).
2. Y. Li *et al.*, Structural insights into immunoglobulin M. *Science* **367**, 1014–1017 (2020).
3. D. A. Calarese *et al.*, Antibody domain exchange is an immunological solution to carbohydrate cluster recognition. *Science* **300**, 2065–2071 (2003).
4. Y. Wu *et al.*, Structural basis for enhanced HIV-1 neutralization by a dimeric immunoglobulin G form of the glycan-recognizing antibody 2G12. *Cell Rep.* **5**, 1443–1455 (2013).
5. C. A. Diebolder *et al.*, Complement is activated by IgG hexamers assembled at the cell surface. *Science* **343**, 1260–1263 (2014).
6. W. B. Williams *et al.*, Fab-dimerized glycan-reactive antibodies are a structural category of natural antibodies. *Cell* **184**, 2955–2972.e25 (2021).
7. K. Imkeller *et al.*, Antihomotypic affinity maturation improves human B cell responses against a repetitive epitope. *Science* **360**, 1358–1362 (2018).

8. I. Kucharska *et al.*, Structural ordering of the *Plasmodium berghei* circumsporozoite protein repeats by inhibitory antibody 3D11. *eLife* **9**, e59018 (2020).
9. D. Oyen *et al.*, Cryo-EM structure of *P. falciparum* circumsporozoite protein with a vaccine-elicited antibody is stabilized by somatically mutated inter-Fab contacts. *Sci. Adv.* **4**, eaau8529 (2018).
10. L. Rougé *et al.*, Structure of CD20 in complex with the therapeutic monoclonal antibody rituximab. *Science* **367**, 1224–1230 (2020).
11. K. Motoki *et al.*, Enhanced apoptosis and tumor regression induced by a direct agonist antibody to tumor necrosis factor-related apoptosis-inducing ligand receptor 2. *Clin. Cancer Res.* **11**, 3126–3135 (2005).
12. T. Tamada *et al.*, TRAIL-R2 superoligomerization induced by human monoclonal agonistic antibody KMTR2. *Sci. Rep.* **5**, 17936 (2015).
13. S. M. Chin *et al.*, Structure of the 4-1BB/4-1BBL complex and distinct binding and functional properties of utomilumab and urelumab. *Nat. Commun.* **9**, 4679 (2018).
14. Y. Yang *et al.*, Tetravalent biepitopic targeting enables intrinsic antibody agonism of tumor necrosis factor receptor superfamily members. *MAbs* **11**, 996–1011 (2019).
15. D. Zhang, M. V. Goldberg, M. L. Chiu, Fc engineering approaches to enhance the agonism and effector functions of an anti-OX40 antibody. *J. Biol. Chem.* **291**, 27134–27146 (2016).
16. M. B. Overdijk *et al.*, Dual epitope targeting and enhanced hexamerization by DR5 antibodies as a novel approach to induce potent antitumor activity through DR5 agonism. *Mol. Cancer Ther.* **19**, 2126–2138 (2020).
17. M. Chodorge *et al.*, A series of Fas receptor agonist antibodies that demonstrate an inverse correlation between affinity and potency. *Cell Death Differ.* **19**, 1187–1195 (2012).
18. G. Robin *et al.*, Restricted diversity of antigen binding residues of antibodies revealed by computational alanine scanning of 227 antibody-antigen complexes. *J. Mol. Biol.* **426**, 3729–3743 (2014).
19. J. W. Stave, K. Lindpaintner, Antibody and antigen contact residues define epitope and paratope size and structure. *J. Immunol.* **191**, 1428–1435 (2013).
20. D. L. Eaton *et al.*, Construction and characterization of an active factor VIII variant lacking the central one-third of the molecule. *Biochemistry* **25**, 8343–8347 (1986).
21. J. Ye, N. Ma, T. L. Madden, J. M. Ostell, IgBLAST: An immunoglobulin variable domain sequence analysis tool. *Nucleic Acids Res.* **41**, W34-40 (2013).
22. H. M. Berman *et al.*, The protein data bank. *Nucleic Acids Res.* **28**, 235–242 (2000).
23. A. Honegger, A. Plückthun, Yet another numbering scheme for immunoglobulin variable domains: An automatic modeling and analysis tool. *J. Mol. Biol.* **309**, 657–670 (2001).
24. J. Dunbar, C. M. Deane, ANARCI: Antigen receptor numbering and receptor classification. *Bioinformatics* **32**, 298–300 (2016).
25. Collaborative Computational Project, Number 4, The CCP4 suite: Programs for protein crystallography. *Acta Crystallogr. D Biol. Crystallogr.* **50**, 760–763 (1994).
26. C. Soto *et al.*, High frequency of shared clonotypes in human B cell receptor repertoires. *Nature* **566**, 398–402 (2019).